International Journal of Thermophysics, Vol. 25, No. 2, March 2004 (© 2004)

Advances in Measurements of the Melting Transition in Non-Stoichiometric UO_2 [1]

D. Manara,[2,3] M. Sheindlin,[2] and M. Lewis[4]

This work presents a study of the melting behavior of the UO_{2+x} system. Self-crucible pulsed-laser melting at high pressure is realized, further improving the recently developed experimental approach. Thermograms of the heated surface of the sample, recorded by a fast pyrometer, show thermal arrests and/or points of inflection corresponding to the phase transformations. A further probe laser beam is focused onto and reflected by the sample surface, and the reflected light intensity is used to detect the exact instants at which melting/freezing transitions occur. Furthermore, a model was developed describing the complex process of laser-induced melting in a system where a solubility gap accompanies the formation of liquid, and a corresponding numerical simulation of the melting-freezing process was performed in order to depict the heat and matter transport phenomena involved. Finally, *liquidus* and *solidus* lines are proposed for the system UO_{2+x} in the range $0 \leqslant x \leqslant 0.21$.

KEY WORDS: hyperstoichiometric uranium dioxide; laser pulse heating; melting; phase diagram.

1. INTRODUCTION

The risk prediction of potential severe accidents in a nuclear plant needs a sound formulation of the equation of state (EOS) for the materials forming the reactor core [1], based on reliable experimental information. In particular, data are needed on the melting transition of the fuel as it defines the integrity limit of the core elements.

[1] Paper presented at the Fifteenth Symposium on Thermophysical Properties, June 22–27, 2003, Boulder, Colorado, U.S.A.

[2] European Commission, Joint Research Center, Institute for Transuranium Elements, P.O. Box 2340, D-76125 Karlsruhe, Germany.

[3] To whom correspondence should be addressed. E-mail: manara@itu.fzk.de

[4] Department of Physics, University of Warwick, Coventry CV4 7AL, United Kingdom.

0195-928X/04/0300-0533/0 © 2004 Plenum Publishing Corporation

Uranium dioxide is the most commonly used nuclear fuel; thus, data on its melting behavior are of great interest. Despite efforts [2, 3] made in the past, its melting behavior has not been determined with sufficient certainty yet, due to the low chemical stability of this compound, especially at high temperature and hyperstoichiometric compositions. In fact, uranium dioxide can easily change its oxidation state in presence of oxygen as it exists over a wide range of compositions UO_{2+x} around the exact stoichiometry.

This work deals with experimental investigations of the melting behavior of UO_{2+x} at several hyperstoichiometric compositions. The basic principles of the method [4, 5] used here are aimed at overcoming difficulties that in the past hindered the only existing measurements by Latta and Fryxell [3], who used a conventional technique. These difficulties were mainly linked to the high, non-congruent evaporation rate, as well as to the contamination of uranium dioxide with the containing crucible material. In a previous study [5], a pulsed laser beam was used to heat part of the sample surface above the melting point, thus avoiding contact of the molten zone with any external contaminant. The specimen was kept under buffer gas at high pressure. Temperature measurements were performed by means of a high-speed pyrometer focused on the sample surface in the center of the laser focal spot. *Solidus* and *liquidus* points were determined visually and by observing the corresponding thermal arrest on the recorded thermograms. However, such an approach still resulted in unreliable points, mainly linked to the nonequilibrium nature of the *overall* melting process. Actually, the inflection point corresponding to the *liquidus* transition was not sufficiently sharp, especially at high oxidation states, and the determination of the *solidus* was even more problematic since no corresponding inflection point could be clearly identified. The interpretation of the thermograms presented another problem. The melting-freezing behavior of a system with a *solidus-liquidus* transition, subjected to fast laser heating (i.e., to high temperature and oxygen concentration gradients) is not straightforward. This issue called for the development of a suitable mathematical model.

2. METHOD

In this work, a novel procedure is implemented, which reduces the mentioned uncertainties. In addition to the information obtained by the thermal arrest observation, a new independent phenomenon is produced and analyzed. A probe laser beam is directed onto and reflected by the sample surface. The resulting reflected intensity permits detection of the exact moments at which melting and freezing occur. Thus, phase transition

points can be detected independently of the complex phenomena, involved in the propagation of the melting-freezing front, occurring in the bulk. In order to corroborate the reliability of the results, it should be verified that the sample composition remains sufficiently stable on the surface during a measurement. To confirm this latter point, a one-dimensional model has been implemented to simulate the pulse-melting experiments.

3. SAMPLES

Nuclear grade urania pellets, fabricated by Advanced Nuclear Materials Co., were annealed in a flux of $Ar + 5\% H_2$ at 1273 K to ensure that their composition was stoichiometric. The sintered density was better than 95% of the theoretical value ($10.95\ g \cdot cm^{-3}$). The O/U atomic ratio determined by thermogravimetric measurements after annealing was 2.00 ± 0.005. The composition was obtained from the change in the sample mass at full oxidation to U_3O_8 in air. Hyperstoichiometric samples were prepared by treating stoichiometric pellets in an Al_2O_3 furnace at different temperatures under a CO/CO_2 flowing mixture of suitable composition, according to the $UO_{2\pm x}$ Ellingham diagram [6]. The final composition was measured by the difference between the sample masses before and after the treatment, and then confirmed by thermogravimetry. The homogeneity of the samples from the surface inward was confirmed through optical and SEM ceramography.

4. EXPERIMENTAL

The experimental apparatus used here is sketched in Fig. 1. The sample is held vertically inside a high-pressure cell. Its lateral surface is wrapped in a teflon ring that prevents the specimen from breaking under the thermal stresses. Pressures of the order of 0.1 GPa prevent evaporation from the specimen surface. Helium was chosen as a filling buffer gas, since it causes the least optical disturbance at high pressures and temperatures. Convective motions in the buffer gas are avoided by placing a thin sapphire protective window 1 mm above the sample surface. Laser beams of two Nd:YAG pulsed-lasers (total power of ≈ 3 kW for several tens of milliseconds) are merged and channeled in the same optical fiber and, hence, simultaneously focused onto the sample surface. The first laser head supplies the "power pulse," heating the sample above the melting point; the second one, separately controlled in intensity and duration, delivers a longer pulse of lower power, ensuring conditioning of the sample cooling rate. In this way, the sample temperature is prevented from decreasing too

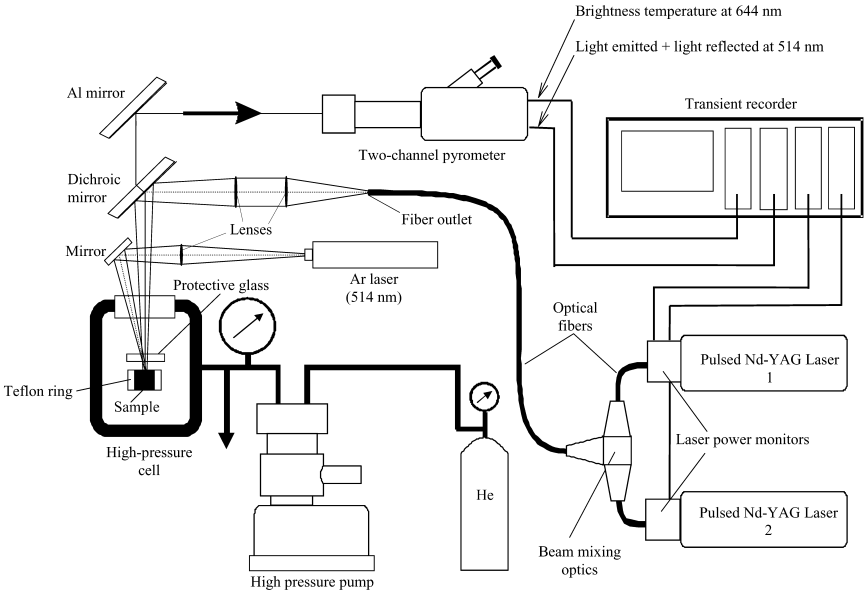

Fig. 1. Equipment employed to measure the melting behavior of stoichiometric and hyper-stoichiometric uranium dioxide.

fast, and undesirable undercooling of the liquid below the freezing temperature is avoided. Due to the random mixing of the laser radiation inside the optical fiber, a homogeneous power density distribution is obtained over the focal spot of 3 mm-diameter. An energy detector placed at the exit of the beam-mixing fiber records the power-time profile of the laser pulse. The temperature of the sample surface heated by the laser beam is measured by a high-speed (total time resolution of 10 μs), two-channel pyrometer [7, 8]. The signals of the pyrometer and of the energy-detector are transferred to a Nicolet Pro 44C Transient Digitizer and to a PC.

The first pyrometer channel, operating at 644 nm and calibrated against a standard gas band-lamp, is used as a temperature reference with an uncertainty better than 0.5% at 2500 K. The obtained brightness temperature is converted into the true temperature by correcting it for the sample emissivity, taken from Ref. 9, and for the total transmittance of the optical path. This latter was directly determined by means of a probe laser.

Furthermore, an Ar probe laser ($\lambda = 514$ nm) is focused on the sample surface in the center of the zone concerned with the melting-freezing process. The fraction of the 514 nm light reflected by the surface and detected by the second channel of the pyrometer (tuned at the same wavelength) depends on the angular reflectivity of the sample. During the

heating stage of an experiment, the first appearance of liquid on the surface causes a sudden change in the angular reflectivity leading to a well defined variation in the light signal. Vibrations of the liquid mass result in oscillations of the reflected light intensity, and both disappear when the freezing point is reached on the cooling phase.

5. SIMULATION OF THE LASER-INDUCED MELTING EXPERIMENTS

A theoretical model was developed at the Joint Institute for High Temperatures of RAS, Moscow, Russia in order to simulate the described laser melting experiments [10]. The model describes a two-component specimen heated from one side by a laser pulse with a known time-dependent power profile. Within a one-dimensional approximation, it permits calculations, by means of a numerical code, of the temperature and composition as functions of time and position in the sample during the pulse, as well as the dynamics of the inter-phase boundary and the depth of the molten zone. The cooling of the material is governed by radiative and convective heat exchange with the surrounding environment. The following approximations are assumed:

(a) The deposited laser radiation is absorbed on the surface.

(b) The maximum surface temperature is much lower than the boiling point. Hence, surface evaporation is assumed to involve heat losses, but not mass losses.

(c) Heat exchange inside the molten pool takes place only by heat diffusion and not by convection. Liquid is assumed to be motionless throughout the experiment.

(d) On the sample rear surface heat exchange occurs through radiation.

(e) Density is temperature-independent.

(f) The material remains two-component throughout the experiment.

A trial *liquidus-solidus* phase diagram is given as an input to the code. According to such a phase diagram, melting can lead to violation of the oxygen homogeneity inside the sample.

The diffusion equation describing the mass transfer within the material is

$$\rho \frac{\partial C_i}{\partial t} + \frac{\partial J_i}{\partial z} = 0 \qquad (i = 1, 2) \tag{1}$$

where t = time; z = depth ($z = 0$ on the heated surface); $\rho = \rho_1 + \rho_2 =$ constant, total material density, and $C_i = \rho_i / \rho$, mass fraction of the component i. The quantity,

$$J_i = -\rho D \frac{\partial C_i}{\partial z} \tag{2}$$

is the diffusion flux; $D = D(C, T)$ is the temperature-dependent effective diffusion coefficient.

By omitting the indices (C and J respectively correspond to the excess oxygen concentration and diffusion flux in the stoichiometric UO_2 matrix), the caloric equation of the heat transfer in the bulk is

$$\rho \frac{\partial h}{\partial t} + \frac{\partial q}{\partial z} + \frac{\partial}{\partial z}\left(J \frac{\partial h}{\partial C} \right) = 0 \tag{3}$$

where $h = h(C, T)$ is the specific enthalpy given as input,

$$q = -\lambda \frac{\partial T}{\partial z} \tag{4}$$

is the conductive heat flux, and $\lambda = \lambda(C, T)$ is the input thermal conductivity.

The last term in Eq. (3) represents the diffusive heat transfer. Conditions (a), (b), (c), and (d) define the boundary conditions for Eqs. (1) and (3). On the solid-liquid interface h and C can undergo a discontinuity (while T remains continuous). The conditions connecting different values ahead of and behind the melting front (indicated by indexes + and −, respectively) moving at a rate v_f, are defined by the energy and mass conservation laws:

$$J^- - J^+ = \rho v_f (C^- - C^+), \tag{5}$$

$$q^- - q^+ + \left(J \frac{\partial h}{\partial C} \right)^- - \left(J \frac{\partial h}{\partial C} \right)^+ = \rho v_f (h^- - h^+). \tag{6}$$

The one-dimensional approximation is acceptable since thermal gradients on the sample surface can be considered mostly axial, and the growth of the crystal upon freezing is columnar, perpendicular to the surface. The meaningfulness of these assumptions can be deduced from the observation of SEM and optical micrographs of sample surface sections after melting. Figure 2 shows SEM micrographs for a stoichiometric sample (Figs. 2a, b), and for a hyperstoichiometric $UO_{2.08}$ sample (Figs. 2c, d). The system can be considered as one-dimensional throughout the melting-freezing process

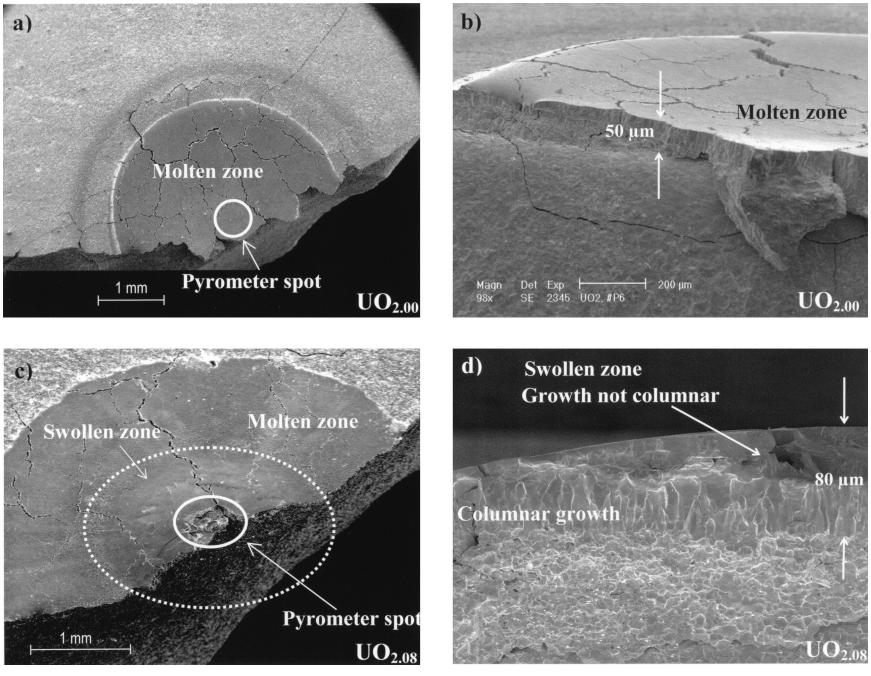

Fig. 2. SEM micrographs of samples subjected to laser induced melting-freezing experiments. (a) and (b): stoichiometric sample ($UO_{2.00}$). (c) and (d): hyperstoichiometric sample ($UO_{2.08}$). Crystal growth in the stoichiometric sample occurs regularly by axial columns. In the hyperstoichiometric sample a swollen zone, where the crystal growth is not columnar, is visible in the center of the molten zone, probably due to displacement of liquid during the inhomogeneous freezing process.

for a stoichiometric sample, where the crystal growth is apparently columnar over the whole re-frozen zone. In hyperstoichiometric samples, instead, a small "swollen" zone in the center of the molten surface is visible, in which the crystal growth was not columnar. The presence of such a "swelling" is probably due to movement of the liquid mass in the radial direction during the solidification process. In this case, a one-dimensional simulation can be justified in the first part of the experiment only, i.e., until the first appearance of solid in the liquid.

6. RESULTS

In the case of a stoichiometric sample, the melting point can easily be determined from observation of the thermal arrest occurring at the freezing temperature on the cooling stage. This confirms that stoichiometric

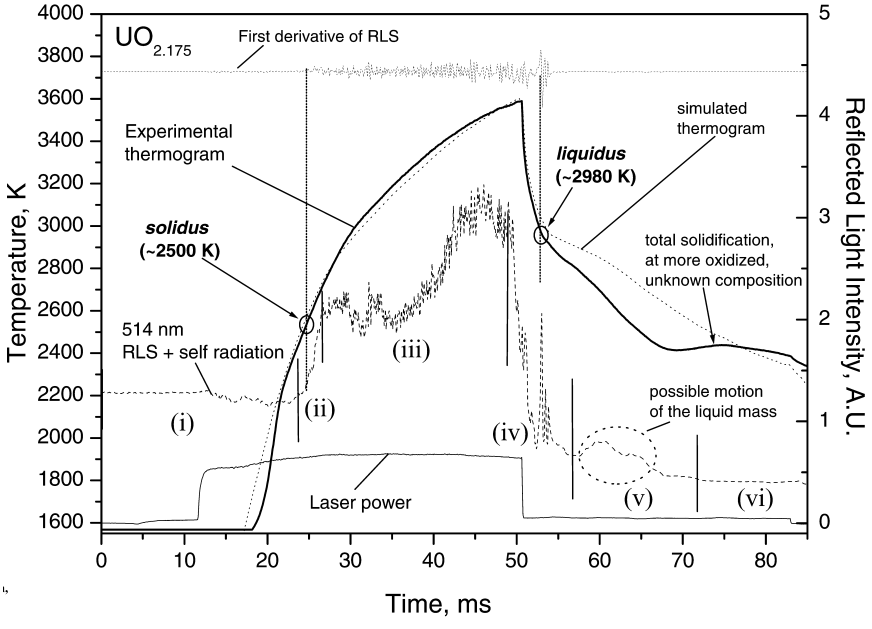

Fig. 3. Experimental and simulated thermograms recorded for a $UO_{2.175}$ sample. 514 nm reflected light signal (RLS) and its derivative are also displayed, with the help of which six stages in the melting-freezing process can be distinguished and *solidus* and *liquidus* transitions determined. Vertical lines across the RLS graph mark the beginning and the end of each one of the six stages.

UO_2 melts congruently, at least as far as it can be established within the precision limits of the method. The process is much more complex for hyperstoichiometric specimens. Figure 3 shows the output of an experiment performed on a $UO_{2.175}$ sample, displaying the typical features of hyperstoichiometric specimens. Here, the thick continuous line is the reference thermogram measured by the pyrometer 644 nm channel. A simulated thermogram is also displayed. The agreement between experimental and simulated curves is acceptable up to the *liquidus* point only, for the reasons explained in the previous section.

On the cooling stage, the 644 nm channel thermogram exhibits a clear inflection corresponding to the *liquidus* transition, and subsequently a significant thermal arrest, which does not show the features typical of a *solidus* transition at the original composition (i.e., a reincrease in the thermogram slope). This latter arrest can be rather attributed to solidification of the remaining liquid (enriched in oxygen), probably frozen in motion. *Solidus* in this case is well determined with the help of the 514 nm reflected light signal (RLS). The first time derivative of the RLS can be used to

more clearly observe the vibrations of the superficial liquid layer. The RLS shows variations of the sample surface state, and, accordingly, six stages are displayed in Fig. 3: (i) The sample surface is not yet molten, and the RLS shows an approximately constant intensity. (ii) A sudden increase in the RLS is observed as the sample surface reaches the *solidus* temperature. An extremely thin, motionless molten layer is formed, acting like a mirror and reflecting a greater part of the Ar laser beam into the pyrometer detector. The RLS reveals the gradual onset of vibrations on the liquid surface. (iii) The amount of liquid produced increases to a point where the molten mass starts vibrating under capillarity forces, and correspondingly it scatters the probe laser beam. The 514 nm signal intensity increases due to the contribution of radiation self-emitted by the hot surface. (iv) The more powerful part of the Nd:YAG laser pulse is turned off, and the temperature decreases very fast (on the order of $10^6\ \mathrm{K \cdot s^{-1}}$). As the solidification front advances, light scattering due to irregular motion of the liquid mass becomes important. Such an irregular motion is cut down when the surface reaches the freezing temperature and the first solid seed is formed, at the *liquidus* temperature (revealed by a spike in the RLS). Correspondingly, a clear inflection is visible on the 644 nm channel thermogram. Superficial vibrations disappear immediately after that, as most of the surface freezes, starting from the first solid nucleus. (v) Inhomogeneous oxygen distribution over the molten mass causes different parts of the pool to solidify at different temperatures, probably leading to a radial displacement of the remaining liquid mass. This can be deduced from the slight variations of the RLS during freezing (between *liquidus* and total solidification). (vi) After complete freezing, vibrations disappear, and the RLS stabilizes around a certain constant level depending on the (new) angular distribution of the reflection. Finally, in spite of disturbing effects of difficult interpretation, both *solidus* and *liquidus* points can be accurately determined from the RLS analysis.

Liquidus and *solidus* points were measured in samples spanning several UO_{2+x} compositions, with $0 \leqslant x \leqslant 0.21$. The resulting phase diagram is shown in Fig. 4. To ensure the accuracy of the measurements, experiments were repeated under different conditions, by changing the intensity and duration of the heating laser beam and the specimen thickness. Measured data were demonstrated to be essentially independent of the buffer gas pressure (see Ref. 5), according to the Clausius–Clapeyron equation. Measurements were also performed on axial sections of the pellets, in order to ascertain that the results were not affected by any inhomogeneous oxygen distribution in the starting composition. Three to ten specimens were investigated for each composition. The horizontal error bands associated with each experimental point represent the uncertainty in the composition

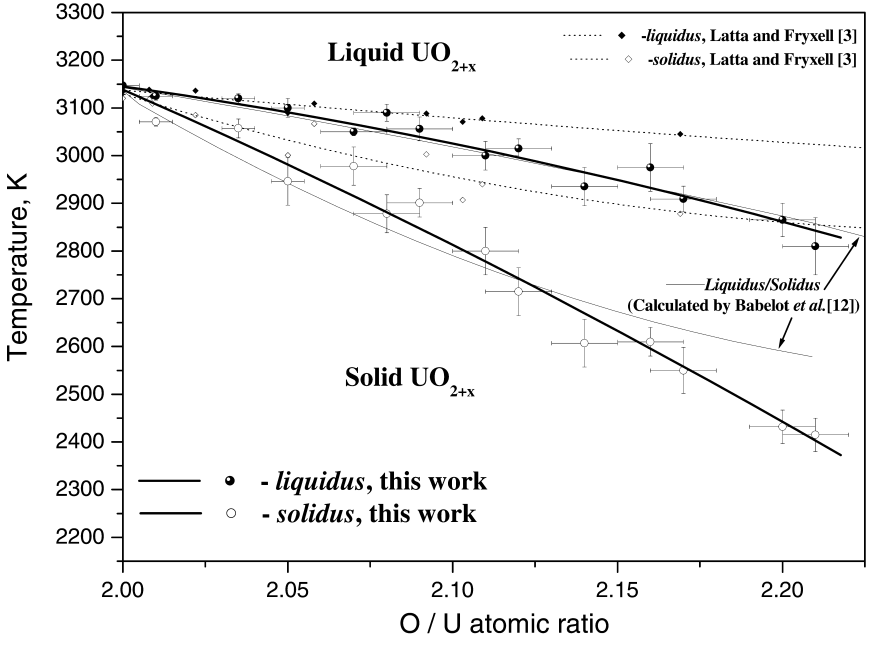

Fig. 4. *Liquidus* and *solidus* lines for the system UO_{2+x} with $0 \leqslant x \leqslant 0.21$: this work (circles indicate the experimental data points, thick continuous lines are a guide for the eye), Latta and Fryxell [3] (diamonds, dotted lines), calculation by Babelot et al. [12] (thin continuous lines).

of specimens; the vertical ones correspond to the standard deviation in the reproducibility of each experimental datum, taking into account also the precision of single measurements.

7. DISCUSSION

Although the measured *solidus* can be regarded as very reliable within the uncertainty given in Fig. 4, the exact composition at which the sample surface reaches the *liquidus* temperature during the cooling stage could be rather uncertain, as important diffusion phenomena from solid into liquid may occur during the experiment. Although the average composition of the overall molten zone was measured by thermogravimetry to be near to the original one, local changes in it are likely to occur during the melting-freezing process. Given the complexity of the system, the simulation presented in Section 4 has to be used to describe how the O/U atomic ratio varies in the liquid as a function of time and position.

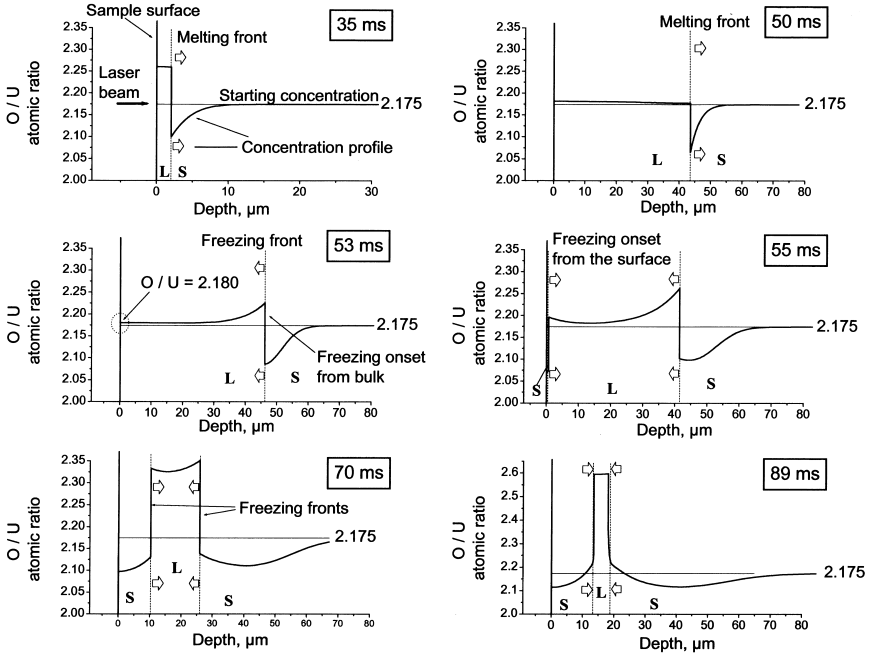

Fig. 5. Oxygen concentration profile and movement of the melting front during a melting-freezing experiment (one-dimensional simulation on a $UO_{2.175}$ specimen). L = Liquid; S = Solid.

Figure 5 shows the calculated one-dimensional concentration profile as a function of the depth z at successive instants in the simulation of the $UO_{2.175}$ experiment of Fig. 3. Due to fast diffusion in the liquid (diffusion coefficients are extrapolated from those recommended in Ref. 11), the composition in the molten phase is approximately constant during the whole melting process. Such composition is richer in oxygen only immediately after the onset of melting, when the molten layer is extremely thin. As the melting front advances, oxygen diffusion tends to restore the original O/U atomic ratio. When the surface reaches the *liquidus* temperature (about 54 ms after the beginning of the experiment in this case), the deviation of the superficial composition from its original value does not exceed the uncertainty in the measured sample O/U atomic ratio.

The solidification process occurs on two freezing fronts: the first starting from the bulk—where solid nucleation takes place more easily—the second, somewhat later, from the outer surface. The liquid phase is richer in oxygen, according to the phase diagram, in proximity of both freezing fronts, but this does not affect the measured transition temperatures. On

the other hand, experiments repeated with different temperature vs. time regimes show that the measured *liquidus* is independent of the measurement duration, indicating that oxygen diffusion proceeds fast enough in the liquid to ensure recovery of the initial composition on the molten surface before the onset of freezing. In conclusion, since no systematic deviation is observed for data points measured under different conditions, the error given in Fig. 4 can be considered as conservative.

In Fig. 4 the *liquidus* and *solidus* lines reported in the literature are compared with those measured in this work. The only experimental curves available were measured by Latta and Fryxell [3]; their temperatures are systematically higher than those presented here, significantly outside the reported uncertainty. However, data measured in [3] for hyperstoichiometric compositions were strongly affected by contamination of the samples with the crucible material (W or Re) and by significant losses of the excess oxygen. Both effects could likely result in liquid formation points higher than those of uncontaminated hyperstoichiometric urania. On the other hand, our lines are in rather good agreement with those calculated by Babelot et al. [12] on the basis of free energy values obtained making use of the Hoch–Arpshofen interaction model [13].

8. CONCLUSIONS

Experimental data on the melting behavior of a complex system such as hyperstoichiometric uranium dioxide have been obtained with an uncertainty about 2% in the worst case. Such data can be used to validate or calibrate advanced equations of state of uranium dioxide providing extrapolations in temperature and pressure ranges which are hardly reachable in laboratory experiments [1].

The method implemented can successfully be used for the experimental study of other high-melting materials and, in particular, provides a powerful tool for investigating the melting behavior of complex, unstable or chemically non-invariant systems undergoing high sublimation or evaporation rates.

ACKNOWLEDGMENTS

The authors are indebted to M. Brykin for developing the numerical simulation of the experiments. Moreover, the authors wish to thank C. Ronchi for his valuable suggestions and for the critical review of the text, and W. Heinz and U. Zweigner for their constant and effective technical support.

REFERENCES

1. I. Iosilevski, G. J. Hyland, C. Ronchi, and E. Yakub, *Int. J. Thermophys.* **22**:1253 (2001).
2. J. A. Christensen, *Stoichiometry Effects in Oxide Nuclear Fuels*, Battle Northwest (USA) Laboratory Report 536 (1967), p. 1.
3. R. E. Latta and R. E. Fryxell, *J. Nucl. Mater.* **35**:195 (1970).
4. D. Manara, C. Ronchi, and M. Sheindlin, *Int. J. Thermophys.* **23**:1147 (2002).
5. D. Manara, C. Ronchi, and M. Sheindlin, *High-Pressure Melting Behaviour of Non-Stoichiometric Uranium Dioxide*, Proc. (on CD) 14th European Conf. Thermophysics, London, September 1–4, 2002.
6. T. B. Lindemer and T. M. Besman, *J. Nucl. Mater.* **130**:473 (1985).
7. M. Sheindlin, *Sov. Tech. Rev. B. Therm. Phys.* **4**:1 (1992).
8. M. Sheindlin and V. N. Senchenko, in *Proc. Int. Symp. on Major Problems of Present-Day Radiation Pyrometry*, Moscow (1986), p. 220.
9. M. Bober, H. U. Karow, and K. Muller, *High Temp.-High Press.* **12**:161 (1980).
10. V. V. Atrazhev and M. V. Brykin, *Numerical Simulation of Melting and Solidification of Binary Mixtures in Laser Heating Pulses (Non-Congruent Phase Transition Solid-Liquid)*, Study Contract No. 17644-2001-03F1SC KAR RU Final Report (2001).
11. W. Breitung, *J. Nucl. Mater.* **74**:10 (1978).
12. J.-F. Babelot, R. W. Ohse, and M. Hoch, *J. Nucl. Mater.* **137**:144 (1986).
13. M. Hoch and I. Arpshofen, *Z. Metallk.* **75**:23 (1984).